

Supporting Information

Self-reconstruction mediates isolated Pt tailored nanoframes for highly efficient catalysis

Yunpeng Zuo, Dewei Rao, Ning Zhang, Tingting Li, Tianyun Jing, Štěpán Kment, Zdenek Sofer, Yang Chai*^a

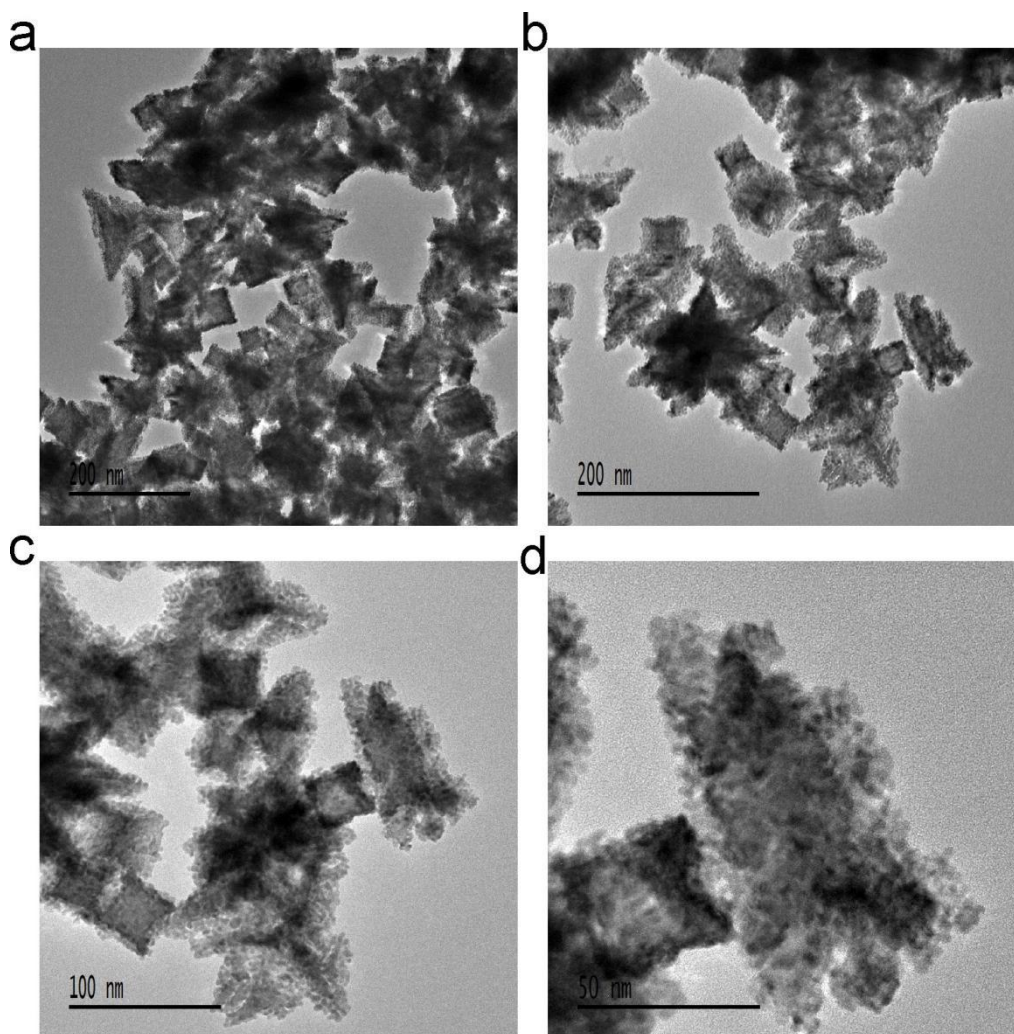


Fig. S1 Morphological characterization of the 3D h-PtPdCu. (a, b) High resolution TEM images of the h-PtPdCu. (c, d) Enlarged HRTEM images. There are many Pt islands covered on the PtPdCu to generated heterostructure. The uniformly dispersed Pt islands can effectively increase the active area of the h-PtPdCu.

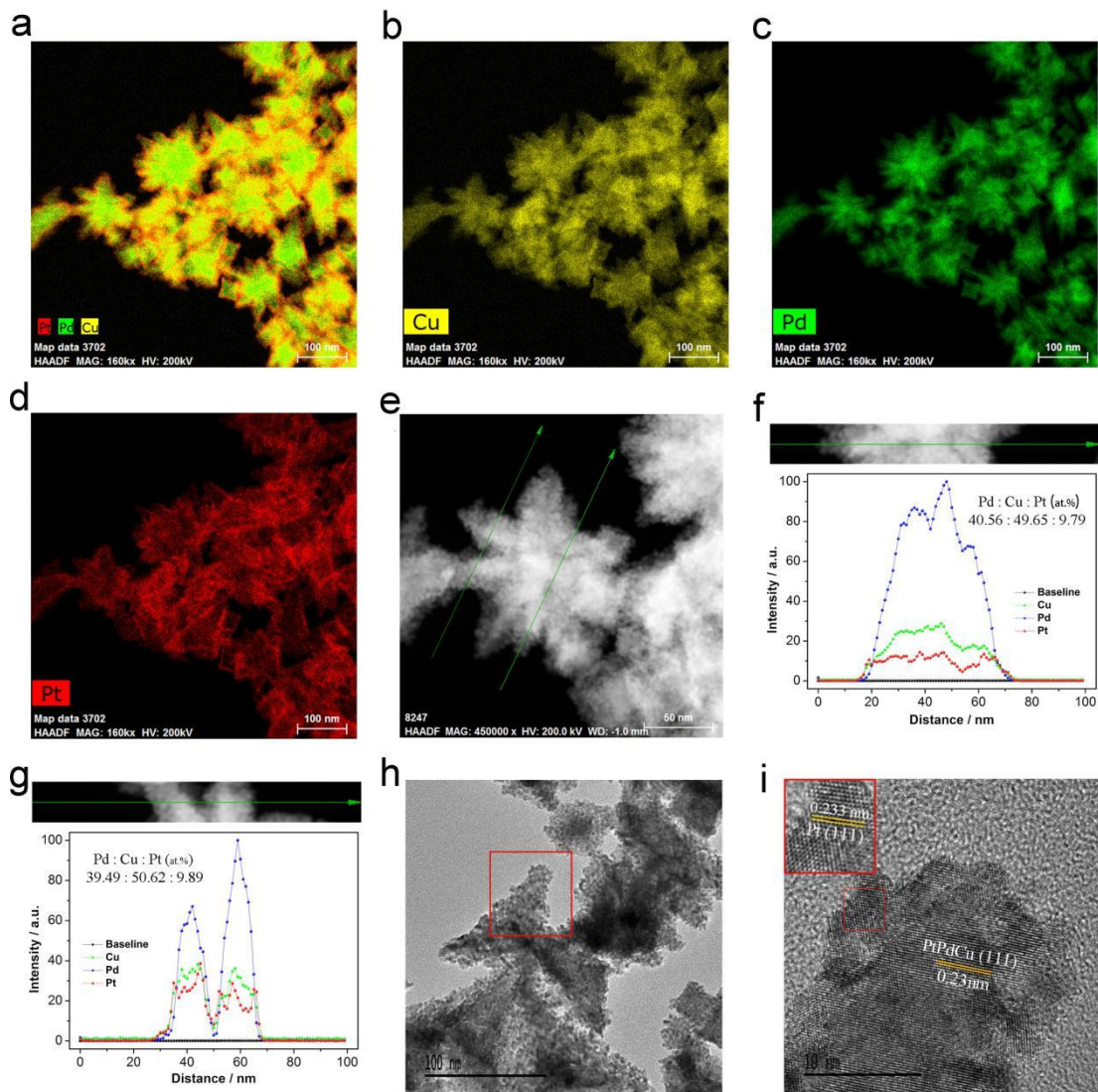


Fig. S2 Structure characterization of the h-PtPdCu. (a, b, c, d) TEM-energy dispersive spectrometer (STEM-EDS) elemental mapping images and (e, f, g) EDS line scanning profiles of the selected directions in a randomly chosen h-PtPdCu. (h, i) Enlarged high resolution TEM (HRTEM) images of the h-PtPdCu.

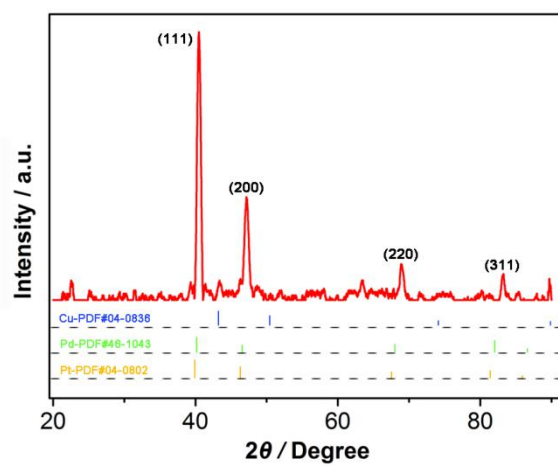


Fig. S3 Powder X-ray diffraction (P-XRD) of the h-PdCu&Pt.

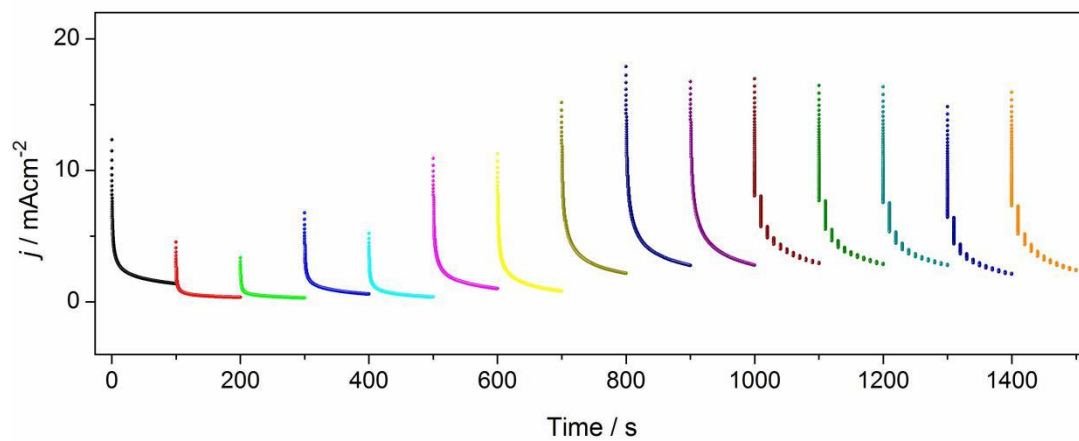


Fig. S4 Chronopotentiometric curves test under 1.0 V vs. RHE with interval of 100 s in 0.5 M H_2SO_4 + 1M $\text{CH}_2\text{OHCH}_2\text{OH}$ solution.

Table S1. The chemical composition of Pd, Cu, Pt of h-PdCu&Pt obtained from the inductively coupled plasma mass spectrometry (ICP-MS).

Elements	Pt	Pd	Cu	Atomic %	ICP-MS
Catalysts					
Content (%)	12.3	63.3	24.4		

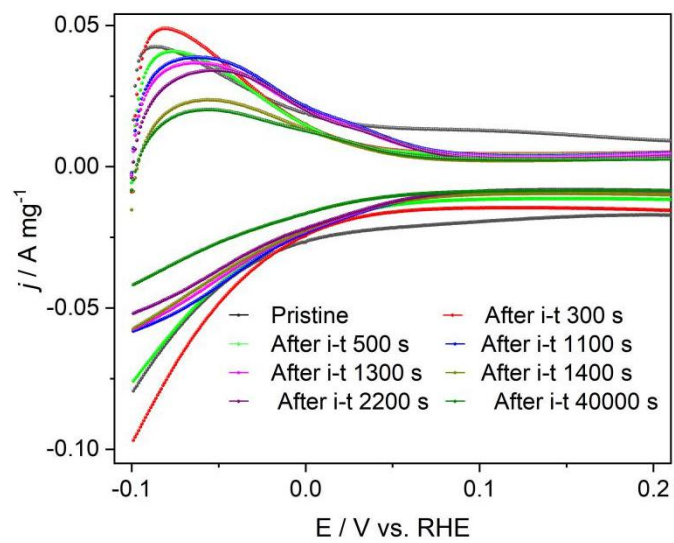


Fig. S5 The cyclic voltammetry of h-PdCu&Pt tested in 0.5 M H_2SO_4 solution with different EGEO reaction time at 50 mV s^{-1} .

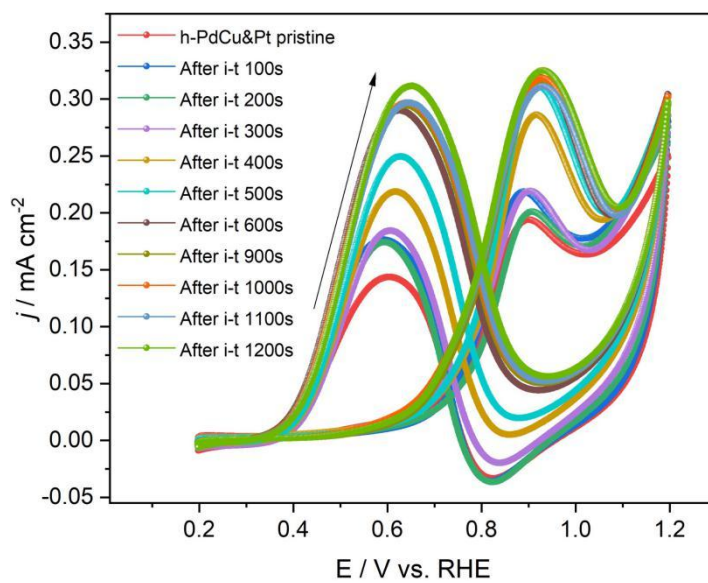


Fig. S6 EGEO of h-PdCu&Pt. The cyclic voltammetry of h-PdCu&Pt tested in 0.5 M H_2SO_4 + 1M $\text{CH}_2\text{OHCH}_2\text{OH}$ solution with different i-t reaction time at 50 mV s^{-1} .

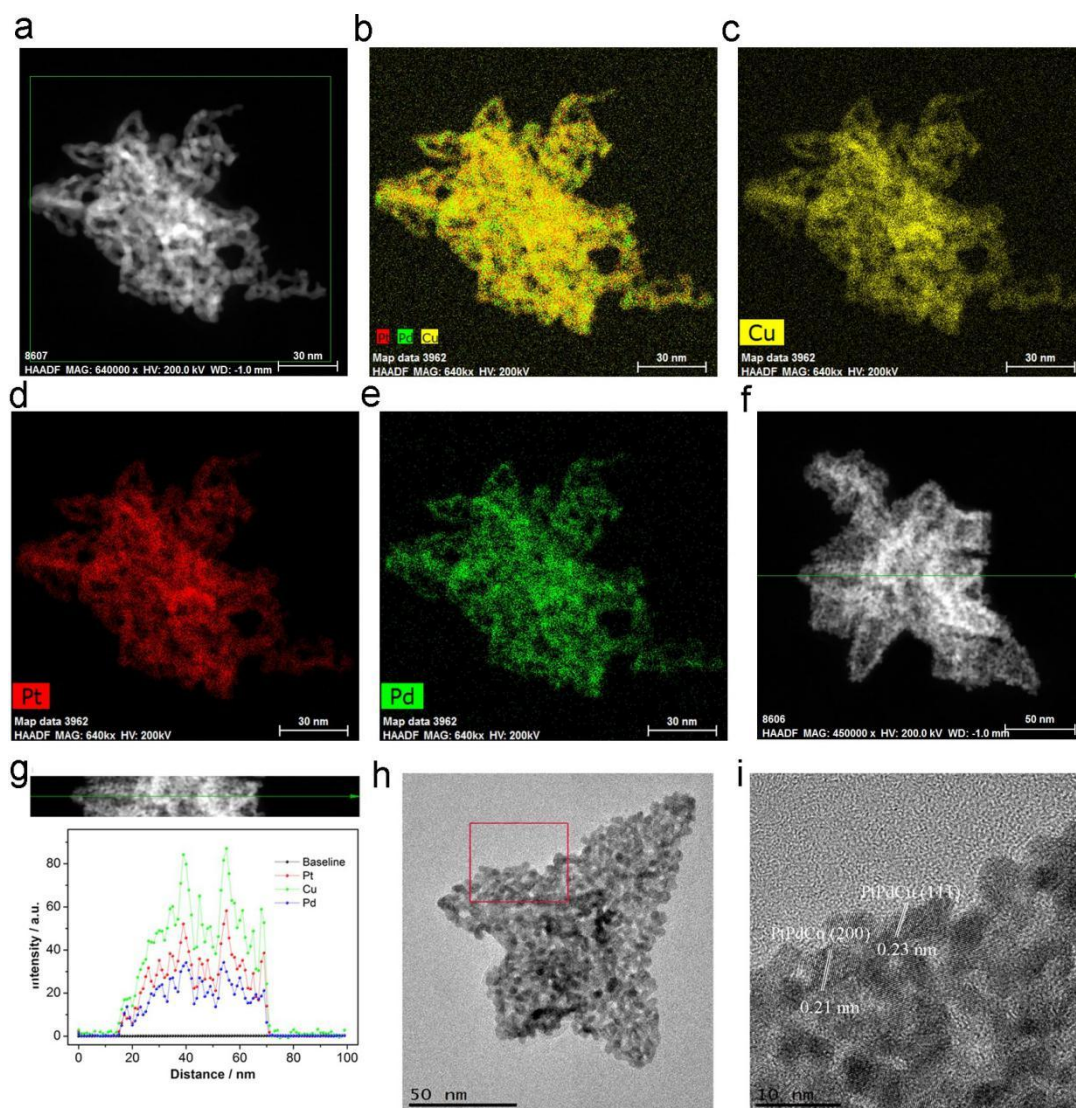


Fig. S7 Structure characterization of the SAPt-PdCu NF. (a, b, c, d, e) TEM-energy dispersive spectrometer (STEM-EDS) elemental mapping images and (f, g) EDS line scanning profiles of SAPt-PdCu NF. (h, i) Enlarged high resolution TEM (HRTEM) images of the SAPt-PdCu NF. The EDS mapping results clearly show that h-PtPdCu gradually change to hollow PtPdCu frame with the structural evolution. Simultaneously, the original heterogeneous structure becomes PtPdCu frame alloy.

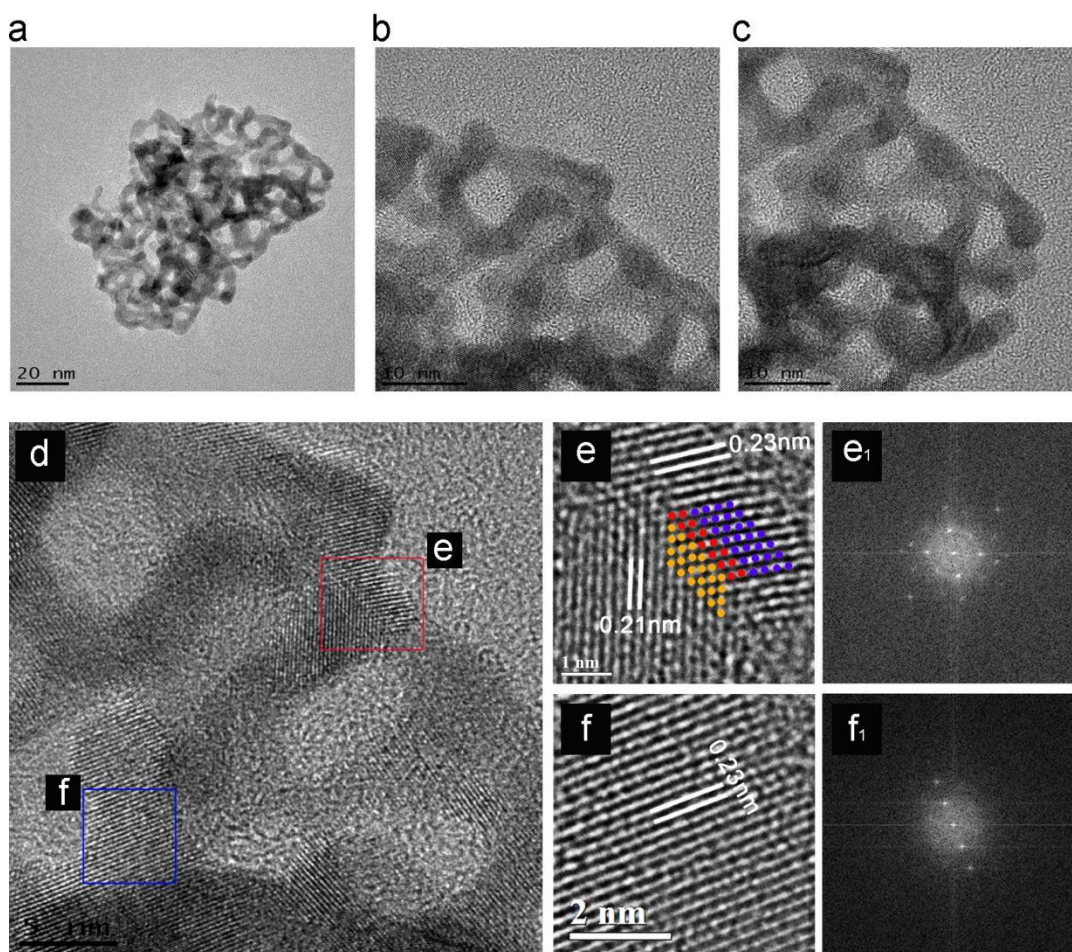


Fig. S8 TEM characterization of the SAPt-PdCu NF. (a, b, c, d) Gradually enlarged TEM images of a representative SAPt-PdCu NF. (e, f) HRTEM images and the corresponding FFTs of the selected area by red and blue squares inserted in (d), respectively. The frame structure has many pores under the size ~ 8 nm, which are 3D accessible for the molecular. There are also abundant unsaturated atoms on the surface of the SAPt-PdCu NF can effectively enhance the activity of the catalyst.

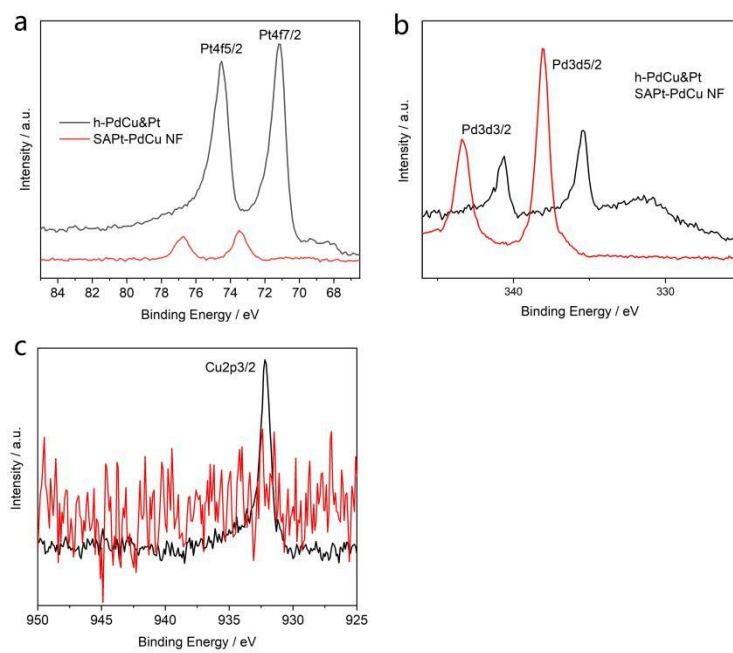


Fig. S9 (a, b, c) High-resolution XPS spectra of Pt 4f, Pd 3d, and Cu 2p.

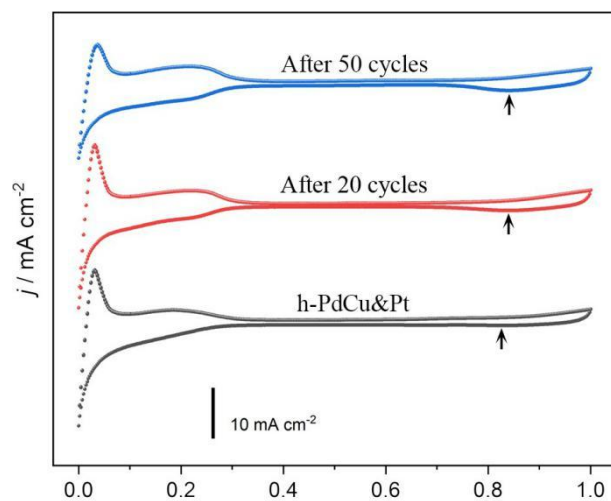


Fig. S10 EGEO CV scanning curves of h-PdCu&Pt under 1, 20, 50 cycles in 0.5 M H₂SO₄ at 50 mV s⁻¹.

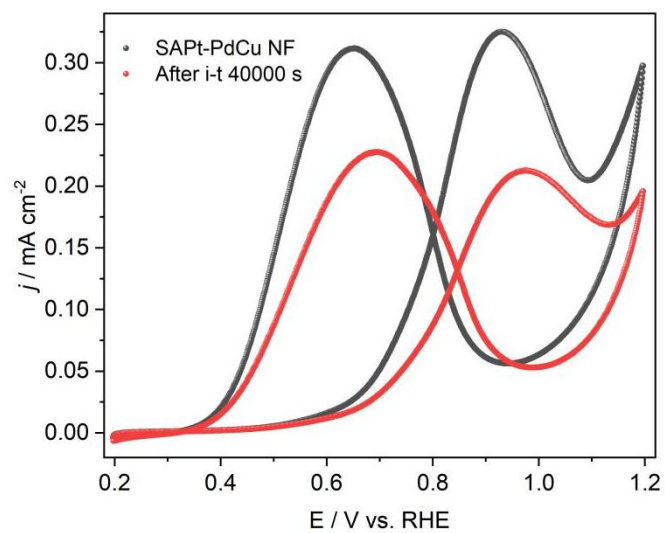


Fig. S11 EGEO CV scanning curves of SAPt-PdCu NF after different i-t stability test.

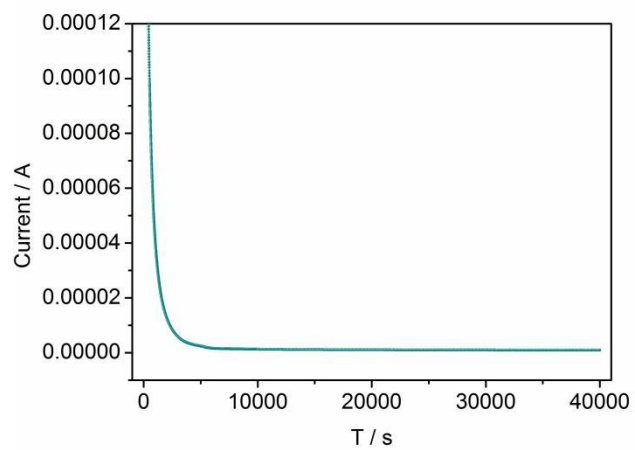


Fig. S12 Chronopotentiometric curves test under 1.0 V vs. RHE for 40000 s in 0.5 M H₂SO₄ + 1M CH₂OHCH₂OH solution.

Table S2. The Pt/Pd/Cu metal ion content in electrolyte before and after EGEO durability test obtained from ICP-MS.

Solution	Elements			mg/L	ICP-MS
	Pt	Pd	Cu		
0.5M H ₂ SO ₄ (before EGEO test)	0.0127	0.0158	0.1197		
0.5M H ₂ SO ₄ (after EGEO test)	0.0115	0.0177	1.6433		

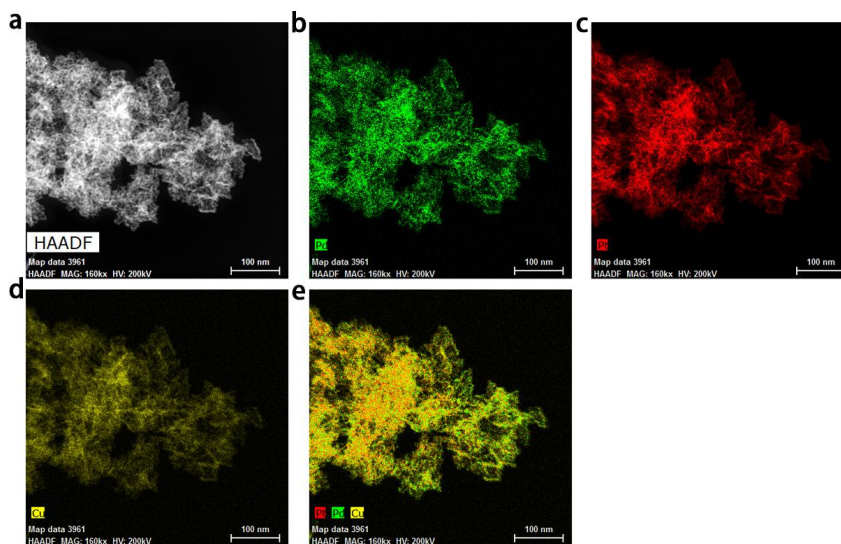


Fig. S13 (a, b, c, d, e) STEM of SAPt-PdCu NF and the corresponding TEM-energy dispersive spectrometer (STEM-EDS) elemental mapping images after stability test.

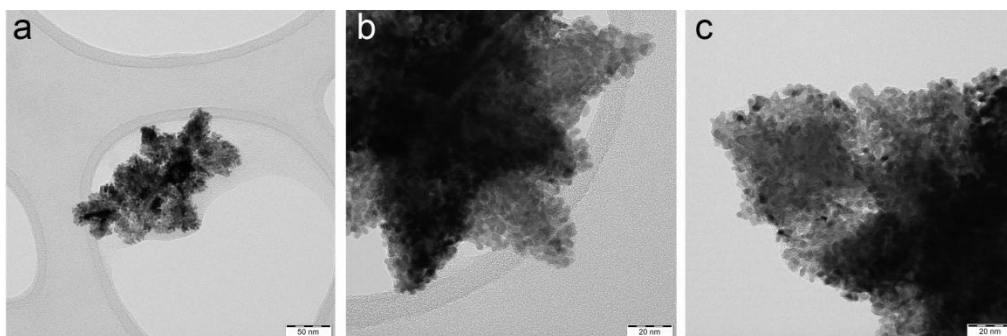


Fig. S14 (a, b, c) TEM images of h-PdCu&Pt after EGEO stability test @ 0.85 V vs. RHE.

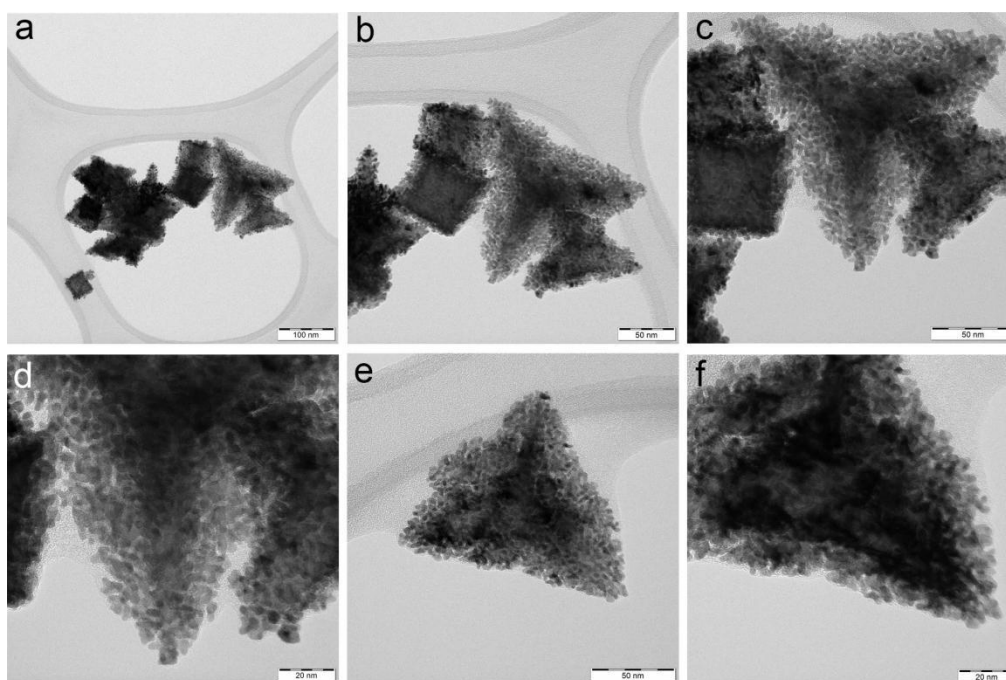


Fig. S15 (a, b, c, d, e, f) TEM images of h-PdCu&Pt after EGEO stability test @ 0.95 V vs. RHE.

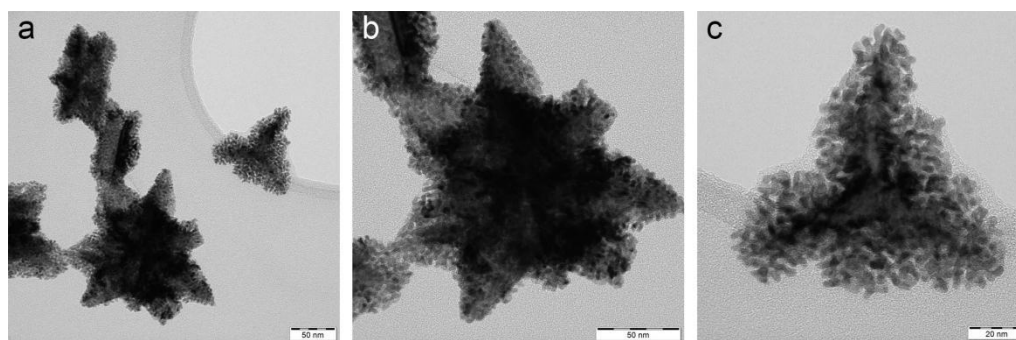


Fig. S16. (a, b, c) TEM images of h-PdCu&Pt after EGEO stability test @ 1.05 V vs. RHE.

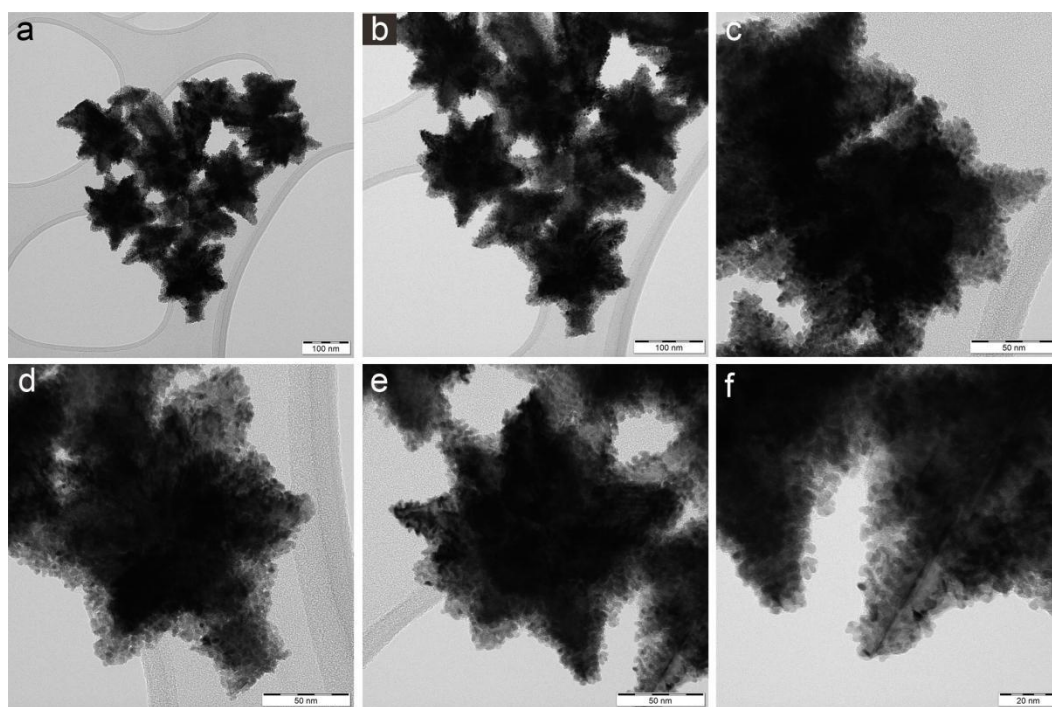


Fig. S17 (a, b, c, d, e, f) TEM images of h-PdCu&Pt after EGEO stability test @ 1.15 V vs. RHE.